IEEE Access
Multidisciplinary ⋮ Rapid Review ⋮ Open Access Journal

Received 23 October 2023, accepted 11 November 2023, date of publication 14 November 2023, date of current version 20 November 2023.

Digital Object Identifier 10.1109/ACCESS.2023.3333251

RESEARCH ARTICLE

Overview of Passive Intermodulation in Modern Wireless Networks: Concepts and Cancellation Techniques

TUHEEN AHMMED[1,2], (Senior Member, IEEE), ADNAN KIAYANI[3], (Member, IEEE), RAED M. SHUBAIR[4], (Senior Member, IEEE), AND HALIM YANIKOMEROGLU[1], (Fellow, IEEE)

[1]Department of Systems and Computer Engineering, Carleton University, Ottawa, ON K1S 5B6, Canada
[2]Ericsson Canada Inc., Ottawa, ON K2K 2V6, Canada
[3]Ericsson AB, 164 80 Stockholm, Sweden
[4]Department of Electrical and Computer Engineering, New York University Abu Dhabi, Abu Dhabi, United Arab Emirates

Corresponding author: Tuheen Ahmmed (tuheen.ahmmed@ericsson.com)

The work of Tuheen Ahmmed was supported by Ericsson Canada Inc.

ABSTRACT Passive Intermodulation (PIM) is a well-known phenomenon that poses a significant challenge to modern wireless communication systems. Although efforts have been made to reduce or mitigate the PIM through hardware design, frequency planning, and/or band separation techniques, the impact of PIM on radio performance remains significant. This is especially true for radio transceivers operating in the frequency division duplex mode, which are known to be susceptible to PIM interference. Moreover, with the adoption of carrier aggregation and advanced multi-antenna technology, PIM is increasingly becoming a major problem in multi-band multi-standard radio systems. Therefore, innovative approaches that exploit PIM detection, avoidance, and cancellation techniques are required to effectively mitigate or reduce its impact. In response to these challenges, this study highlights various PIM interference mechanisms and their interactions which cause potential receiver sensitivity degradation. The discussion further explores PIM mitigation strategies, and underscores the potential of digital PIM cancellation solutions to offer a hardware-independent resolution for reducing PIM impact in multi-band radios, in the 5G era and beyond in radio systems.

INDEX TERMS 5G new radio (NR), base station (BS), carrier aggregation (CA), digital cancellation techniques, frequency division duplex (FDD), interference, multiple-input multiple-output (MIMO), passive intermodulation (PIM), passive intermodulation cancellation, signal-to-noise ratio (SNR).

I. INTRODUCTION

Wireless networks have undergone significant evolution since their inception, with each subsequent generation introducing innovative technologies to improve transmission data rates and quality. To meet the growing capacity and throughput requirements, new technologies such as Long Term Evolution (LTE)-Advanced and fifth-generation (5G) new radio (NR) have introduced carrier aggregation (CA), higher-order modulation, and multiple-input multiple-output (MIMO) techniques [1], [2], [3], [4].

In particular, CA technology enables flexible transmission and reception across multiple parts of the spectrum simultaneously, facilitating wider transmission bandwidth utilization to achieve higher data rates. It improves spectrum utilization by combining spectral resources from within the same band (intra-band CA), both contiguously and non-contiguously, and across multiple bands (inter-band CA) [5], [6], [7].

Furthermore, in the context of 5G, the spectrum has expanded, and two frequency ranges have been defined. Frequency range 1 (FR1) includes all the existing and new

The associate editor coordinating the review of this manuscript and approving it for publication was Hosam El-Ocla.

bands from 0.41 GHz to 7.125 GHz, while frequency range 2 (FR2) encompasses new bands from 24.25 GHz to 52.6 GHz as FR2-1 as well as bands from 52.6 GHz to 71 GHz as FR2-2 [1], [5], [8]. 5G NR also requires dual-connectivity (DC) to enable user equipment (UE) to connect to both LTE and NR cells simultaneously in non-standalone (NSA) 5G networks. This enables the transmission and reception through both LTE and NR carriers, utilizing LTE mid-band frequencies for enhanced coverage along with NR FR2 frequencies for higher data rates. This approach significantly improves network performance and efficiency [3], [9], [10], [11], [12].

As we move towards future sixth-generation (6G) wireless networks, it is expected that a wide range of frequencies will be utilized, including an additional millimeter wave range and THz band (0.1 THz - 10 THz) frequencies. This is because emerging applications such as virtual/augmented reality, autonomous driving, Internet of Things (IoT), and wireless backhaul will require even higher data rates and lower latency. Furthermore, the widespread adoption of artificial intelligence (AI) has also been anticipated in both 5G-Advanced and 6G networks. This includes improving the performance of 5G NR air interface, and incorporating integrated AI and communication in the forthcoming 6G [13], [14], [15], [16], [17], [18]. The ultimate objective is the seamless integration of 5G, 5G-Advanced, and earlier technologies within 6G wireless networks.

In summary, low-, mid-, and high-band frequencies, along with modern technologies, are being utilized to accommodate higher data rates. However, with these advancements, the network is becoming more complex, and the complexity of transceiver design is also increasing. From the perspective of cellular system implementation, radio frequency (RF) imperfections arising from component non-idealities pose a significant challenge. Among the different RF degradation effects, intermodulation distortion (IMD) is particularly problematic as it can severely constrain system performance.

IMD typically occurs when different frequency signals pass through a nonlinear system, resulting in unwanted spectral emissions. In general, both active and non-active (passive) components of a radio system can generate IMD, and their relative power depends on the linearity characteristics of a component. On the transmitter (TX) side, nonlinear distortion in the TX power amplifier (PA) results in spectral regrowth, causing adjacent channel interference [19], [20], [21]. In CA, when radio transceivers operate in the frequency division duplex (FDD) mode, managing the spectrum regrowth of the modulated TX signal can be challenging, as the duplex spacing can be significantly reduced. Consequently, out of band emission (TX noise) can potentially leak into the receiver (RX) chain and may result in sensitivity degradation. Furthermore, the TX nonlinearities for non-contiguous carriers can introduce IMD directly in the RX band, overlapping with the received signal, and causing RX desensitization [20], [22], [23]. The presence of a TX leakage signal at the RX input can trigger additional RX nonlinearities, such as the generation of IMD products from TX leakage in an RX low-noise amplifier or the mixing of a TX leakage signal with an interferer signal, ultimately degrading the RX signal-to-noise ratio (SNR) [24], [25].

When the source of IMD generation is a passive RF component, it is referred to as passive intermodulation (PIM) [26], [27], [28]. In a high-power multi-band FDD radio, ferromagnetic materials or other physical mechanism, such as metal oxidation or mechanical disturbances of passive components, can cause nonlinear effects. However, the source of PIM is not limited to components inside a transceiver; any passive component along the transmission signal path can cause PIM. For example, a metal fence in the vicinity of an antenna that is part of the built environment of a radio site can also contribute to PIM. Although unwanted TX distortion products can potentially be filtered out by cavity filters in a radio, PIM interference is generated inside or after the filter and cannot be eliminated. The 3rd Generation Partnership Project (3GPP) Technical Specification 37.808 V12.0.0 (2013-09), Release 12, recognizes that the PIM can cause extreme RX performance degradation in BS radio systems, with several FDD band combinations being identified as susceptible. In addition to configured FDD bands in a radio transceiver, PIM may also be reflected within the site and coupled into an operator's co-located Time Division Duplex (TDD) band, causing desensitization. For instance, the passive harmonic distortion of 5G NR n3 overlap with 5G NR n78 band [22], [29]. Similarly, PIM can potentially be an issue for asynchronous TDD operations when one base station (BS) is transmitting while the other is receiving simultaneously.

Hence, it can be concluded that PIM represents a major interference problem in modern radio systems. This interference leads to an elevated RX noise floor, resulting in RX desensitization, reduced cell coverage, or potentially rendering the entire transmission link inoperable [30], [31]. In addition to its impact on radio design and configuration, PIM interference also presents significant challenges for network planning and operation. This challenge is particularly pronounced in scenarios involving energy-efficient buildings and indoor deployments. As a result, eliminating PIM entirely from radio networks is often impossible [32].

Accordingly, this study attempts to highlight the PIM issue in 5G and beyond wireless systems. In contrast to the existing literature, which addresses specific PIM challenges, the main contributions of this study can be summarized as follows:

- A comprehensive overview of the PIM interference mechanism in LTE-Advanced and 5G radio systems is provided. This includes the classification and elaboration of major PIM sources to facilitate the design process of radio transceiver systems and networks.
- The impact of PIM on radio system performance is demonstrated through practical real-world 5G network deployment examples.
- Behavioral models for nonlinear systems are discussed, with an emphasis on memoryless nonlinear systems and systems with memory effects. The subsequent section

presents the application of these models to capture the effects of PIM.
- An in-depth discussion of the potential of digital cancellation techniques for PIM is presented among several highlighted approaches for PIM mitigation. This exploration is supported by the presentation of actual RF measurement results obtained using commercial multi-band high-power MIMO FDD radios.

II. REVIEW METHODOLOGY

The primary objective of this study is to assess the impact of PIM on wireless communication systems and explore PIM mitigation techniques. To achieve this, we conducted a systematic review by referencing an extensive range of sources, including scholarly articles, journal publications, academic publications (including Masters and PhD theses), 3GPP specifications, and patents. This systematic approach fully addresses this problem and minimizes potential bias, thereby enhancing the reliability of our findings. The rigorous methodology adopted suits our goal of a comprehensive assessment of PIM.

We employed a meticulous search strategy, utilizing keywords and search strings (e.g., PIM, PIM cancellation, PIM mitigation, digital self-interference cancellation, PIM plus machine learning) across multiple databases, including IEEE Xplore, arXiv, and Google Scholar. We also applied key terms and queries to explore Google Scholar and Google Patents, targeting articles from various journals dedicated to PIM research and PIM cancellation.

Starting with an initial pool of sources from 1990 onwards (beginning with P. Lui's pioneering work [26]), we meticulously screened over 300 papers. We then conducted a rigorous review to identify articles that focused on behavioral modeling and digital PIM cancellation techniques. This selection was further refined to 150 articles, offering a comprehensive basis for systematic analysis and an in-depth understanding of the recent literature on digital PIM cancellation techniques. We placed particular emphasis on studies that employed quantitative methodologies to enhance the depth of insight into this field.

III. PASSIVE INTERMODULATION (PIM) CONCEPTS

Intermodulation (IM) is a phenomenon that occurs in wireless communication systems when two or more signals of different frequencies pass through a device that exhibits nonlinear behavior. The output of a nonlinear system can then contain additional unwanted signals, commonly called spurious signal components or spurious emissions, which are produced by the sum and difference of the original signal frequencies.

PIM in wireless systems generally arises when a high-power transmit signal traverses a passive device in its transmission path. Typical PIM sources in a radio transceiver include cables, connectors, duplex filters, and antennas. In this context, loose mechanical junctions, inconsistent metal-to-metal contacts between RF connectors, corrosion, loose cable connections, dirt in connectors, temperature variations, sharp edges in connectors, paint with ferrite filler, and surge protection devices on a BS can trigger PIM [27], [33]. Moreover, PIM can also originate from external objects in the antenna's radiation field, such as metal fences in the site's built environment [21], [28], [33], [34].

In addition to the power of the transmit signal, PIM usually becomes relevant with configuration of TX and RX frequencies. Depending on the uplink (UL) and downlink (DL) frequency allocation in an FDD network, the spurious IM products of the transmit signal created by the PIM may fall within the passband of the RX. Consequently, PIM-induced distortion can elevate the RX noise floor and may lead to RX desensitization.

To achieve a deeper understanding of PIM, the generation of IM products should first be discussed. In general, a system is characterized by its input-output relationship. A linear system generates an output that is directly proportional to the input, implying that the output is the algebraic sum of the input. However, a nonlinear system diverges from linear properties. The nonlinear behavior of a passive device can be mathematically described using a power series

$$y = \sum_{k=0}^{\infty} a_k x^k, \tag{1}$$

where x and y represent the input and output signals of a nonlinear device, k is the order of the power series, and a_k is the coefficient of the power series terms [24], [35].

According to (1), when a single fundamental frequency (f_1 or f_2) is input to a nonlinear device, harmonic signals are generated and appear in the output as integer multiples of the fundamental frequency ($2f_1$, $3f_1$, $4f_1$, etc., or $2f_2$, $3f_2$, $4f_2$, etc.). The amplitudes of harmonics typically decrease as their order increases. However, harmonic signals are unwanted and can cause interference in wireless systems. When the two fundamental frequencies f_1 and f_2 pass through a passive nonlinear system as an input, the output consists of both harmonic and IM signals (products) due to the combination of f_1 and f_2, as described by (1). The general representation of these signals is as follows

$$f_{IM} = |\pm nf_1 \pm mf_2|, \tag{2}$$

where f_{IM} is the IM product frequency and n and m are integer coefficients. The absolute values of these coefficients $|n + m|$ are known as the orders of the IM products. IM products are also unwanted signals and can cause significant interference, leading to reduced system efficiency and decreased performance [24], [26], [36], [37], [38], [39]. This theory also applies to multi-carrier systems that operate in different frequency bands. For example, three frequency components can produce 3rd order IM (IM3) products, such as $\pm f_1 \pm f_2 \pm f_3$.

The range of IM products expands with higher-order IM. When the fundamental frequencies have the same bandwidth, the range of the IM products is determined by multiplying the

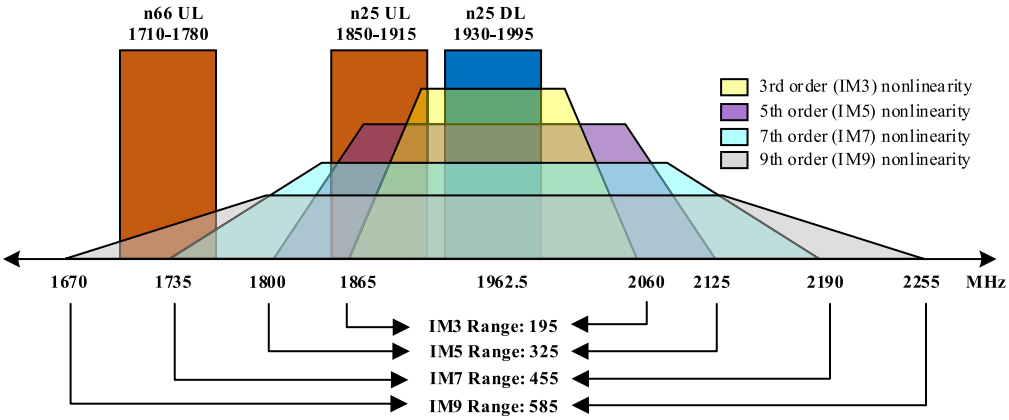

FIGURE 1. Intermodulation distortion on a 5G NR dual band (n25 n66) high-power MIMO FDD radio. The TX signals from n25 traverse through nonlinear components of the radio which generates intermodulation products on the RX bands, and possibly impacting the actual RX signals.

bandwidth of the fundamental frequency by the IM product order number. However, if the fundamental frequencies have different bandwidths, the range of the IM products can be obtained as follows:

$$R_{IM} = |n|BW_1 + |m|BW_2, \tag{3}$$

where R_{IM} is the range of the IM product, BW_1 and BW_2 are the bandwidths of the fundamental signals, and n and m are integer coefficients used in (2) [21].

As the input power in the radio system increases, the amplitudes of the IM products also increase. Specifically, a 1 dB increase in the input power can theoratically result in a 3 dB increase in the amplitude of the IM3 product [21], [26], [27], [28]. Among the IM products, IM3 ($2f_2 - f_1$ and $2f_1 - f_2$) has the greatest impact on the system because of its higher amplitudes compared to the others and its proximity to the fundamental frequencies.

Fig. 1 illustrates the impact of an IM on a 5G NR dual-band (n25 n66) high-power MIMO FDD radio. The illustration displays various IM products (IM3, IM5, IM7, and IM9) with ranges of 195 MHz, 325 MHz, 455 MHz, and 585 MHz, respectively. It is evident that the IM range increases with higher-order IM. Higher-order IM, such as IM7 and IM9, affects not only n25 UL but also n66 UL.

It is worth noting that the example illustration assumes the entire DL bandwidth utilization to signify the reach of IMD when DL carriers are allocated at the band edges. The specific bandwidth of IMD scales with the carrier bandwidth and can be determined according to (3). Furthermore, the power spectral density (PSD) of an IMD at a given transmission power is spread over its bandwidth. Consequently, narrower carrier bandwidths lead to narrower but higher spectral IMD components [40], [41], [42].

IV. CLASSIFICATION OF PIM SOURCES

In this section, we explore the sources of PIM nonlinearity. As previously mentioned, PIM can originate from various factors. Our objective is to categorize these diverse sources into two broad groups. Furthermore, we conclude this section by presenting a table that lists common internal and external PIM sources. This resource can be invaluable for radio transceiver design and deployment to prevent, diagnose, and troubleshoot PIM related issues.

A. CONTACT AND MATERIAL NONLINEARITY

Based on physical phenomena, PIM sources can be classified into two categories: *contact nonlinearity* and *material nonlinearity*.

Contact nonlinearity occurs when current flows through junctions between different materials, resulting in nonlinear behavior. Nonlinearity can be generated at any contact point between metals, such as metal-metal and metal-insulator-metal junctions. Oxidized and contaminated metallic joints also contribute to this type of PIM. Examples in this group include connections between waveguides, cable connectors, duplexers, attenuators, terminations, and antennas [24], [43], [44], [45], [46], [47], [48], [49], [50], [51], [52].

Material nonlinearity refers to the nonlinear current response of materials to an applied voltage. This behavior is associated with the conductive, dielectric, and magnetic properties of materials. Ferromagnetic materials, such as iron and nickel, are included in this group, as well as ferrimagnetic materials found in isolators, circulators, resonators, and phase shifters. These materials are important sources of PIM [24], [44], [45].

B. INTERNAL AND EXTERNAL

Based on physical location, PIM sources in BS radio systems can be classified into two categories: *internal* and *external*.

Internal sources refer to passive components in the radio transceiver RF chain, such as transmission lines, connectors, and antennas. In contrast, *external sources* are beyond the antenna and transmission paths. They originate from the surrounding environment and are often caused by nonlinearities in nearby metallic objects, such as billboards, metal fences, or any other metallic object that can reflect

TABLE 1. Common internal and external PIM sources.

Internal Sources	External Sources
Antennas	Tower modules and components
Connectors	Brackets
Diplexers	Metallic objects and obstacles
Duplexers	Air conditioning vents
Loose connections	Billboards
Tower mounted amplifiers	Rooftop lighting
Filters	Wire fences
Cables	Bolts

or scatter signals [28], [34]. For instance, a corroded metal object near an antenna can reflect a transmitted signal and generate PIM. This phenomenon is known as the Rusty Bolt Effect [34], [53], and rusty metallic objects, such as mesh fences and drain pipes can be sources of IM [21], [33].

Table 1 provides a list of common internal and external PIM sources.

V. IMPACT OF PIM ON RADIO PERFORMANCE

FDD is a widely adopted duplexing scheme for FR1 bands, in which a paired spectrum for simultaneous transmission and reception at different RF frequencies is used [6], [7], [54]. A duplexer is used to connect the TX and RX RF chains to a common antenna, which prevents the strong transmitted signal from affecting the RX side. Typically, two bandpass filters are used within a duplexer to suppress TX noise from leaking into the RX and to block out-of-band interferers. However, due to the finite filter isolation between the TX and RX, there can still be an effect on the RX from the transmitted signal. Moreover, achieving large isolation between the TX and RX ports of the duplexer is less desirable because of the associated size, cost, and design challenges [20], [42], [55], [56], [57], [58].

Among the other RF challenges, PIM also represents a major challenge for wireless communication systems for high-power FDD radios [21], [39], [41], [59], [60]. In general, under high-power conditions, the linearity characteristics of the passive RF components in the radio can easily be changed [60], [61]. Modern single-band multi-band radios commonly use 60 watts per RF port, resulting in a total power of 240 watts for a radio of four RF ports.

In addition to the higher transmit power, the employment of more carriers through CA, wider transmission bandwidths, and more configured bands per radio can further complicate PIM issues and make it a more persistent problem for multi-band radios [62], [63]. As the number of carrier frequencies increases, the number of PIM products falling within the RX band could also increase rapidly. For instance, when seven carriers are simultaneously present in a TX-RX antenna, the number of possible 3rd order PIM components can reach up to 100 [26], [39]. Moreover, the risk of excessive PIM distortion increases as antenna systems become more complex [45].

Typically, the power of IM products is lower than that of the fundamental transmitted frequencies. However, it can still be significant relative to the received UL signal power, potentially causing RX sensitivity degradation [29], [64], [65]. The received signal strength of a power limited cell edge user can generally be very low, and it may be negatively affected by the presence of PIM. For instance, GSM specifications mandate that IM products within the RX band should not exceed -103 dBm, but the practical requirement is more stringent, ranging between -110 and -115 dBm [39]. Thus, PIM significantly affects the RX performance and can cause a sensitivity degradation of more than 10 dB in the worst case [27].

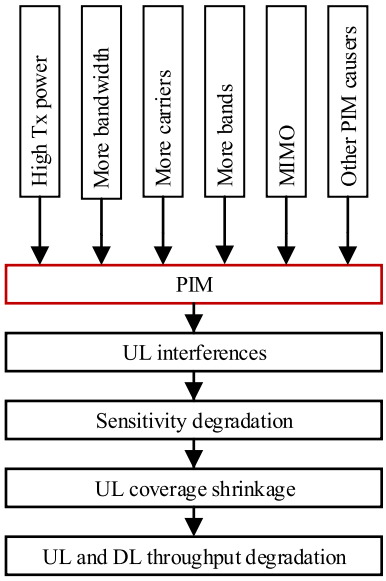

FIGURE 2. Impact of PIM in radio networks.

Fig. 2 illustrates the primary causes of PIM, encompassing factors such as higher TX power per RF port, increased bandwidth, and other PIM sources. It also demonstrates the resultant impact on the RX sensitivity, which leads to reduced UL coverage and overall throughput degradation in radio networks.

The impact of PIM can also be characterized in terms of reduction in the SNR, which is a key performance indicator in wireless communication systems. When the PIM level exceeds the noise floor of the system, the SNR could be significantly reduced. In fact, a 1 dB decrease in SNR can lead to an approximately an 11% reduction in channel capacity [24].

Finally, in terms of managing and mitigating PIM, PIM detection in live networks is challenging and expensive because on-site visits are often required. Traditionally, operators rely on highly skilled technicians and sophisticated tools to identify and locate sources of PIM nonlinearity [66]. Nevertheless, as mentioned earlier, it is often impossible to fully mitigate the impact of PIM.

VI. PIM CALCULATION AND VISUALIZATION

In this section, the two prevalent types of PIM—*internal* and *external*—are being discussed, calculated, and visualized

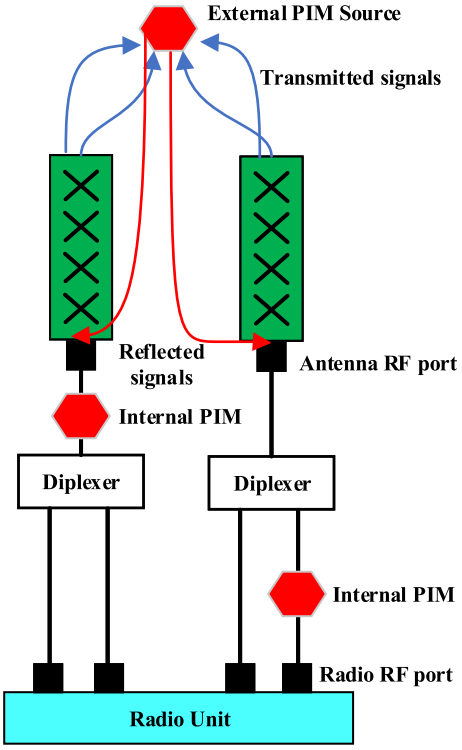

FIGURE 3. Internal and external Passive Intermodulation (PIM) in radio systems.

within the context of a 5G NR dual-band (n25 n66) high-power MIMO FDD radio system.

Internal PIM, which is sometimes referred to as transmission line PIM, occurs when DL signals from the same antenna branch cause interference with the UL frequency of that particular branch. This interference is caused by passive nonlinearities within the same transmission line, as shown in Fig. 3. The figure illustrates internal PIMs between the antenna RF port and diplexer, as well as between the diplexer and radio RF port. In this context, a diplexer refers to a passive RF filter with multiple ports, which allows the sharing of a common antenna between two distinct frequency bands.

External PIM, also referred to as air-induced PIM [22], [56], [65], [67], occurs when DL signals from the same or different antenna branches cause interference with the UL frequency of any branch. This type of PIM is primarily caused by elements located outside the radio unit, as illustrated in Fig. 3. In this figure, the transmitted signals (blue) from the BS antenna are reflected on an external PIM source, and the reflected signals (red) impact any or all of its RF branches.

The concept and calculation of internal and external PIM in a real-world 5G NR network are demonstrated through an example of a dual-band high-power MIMO FDD radio. The radio supports two NR frequency bands, n25 and n66, with the first four branches dedicated to n25 and the next four branches dedicated to n66 for both the UL and DL. As a result, the radio has the capabilities of four TXs and four RXs. When considering the impact of PIM, the entire band is considered to illustrate how any channel bandwidth within the range, such as 20 MHz, 40 MHz, 60 MHz, etc., is affected by PIM. This example focuses specifically on IM3 and IM5.

TABLE 2. Spectrum of a 5G NR dual band (n25 n66) high-power radio.

Band	Direction	Frequency Range (MHz)	Bandwidth (MHz)
n66	Uplink	1710–1780	70
n25	Uplink	1850–1915	65
n25	Downlink	1930–1995	65
n66	Downlink	2110–2200	90

The spectrum details of the radio are presented in Table 2 and are visualized in Fig. 4. The figure illustrates the duplex spacing, which represents the difference between the DL and UL frequencies, is 400 MHz for n66 and 80 MHz for n25. Additionally, it shows a band separation of 70 MHz between n66 UL and n25 UL, 15 MHz between n25 UL and n25 DL, and 115 MHz between n25 DL and n66 DL.

A. INTERNAL PIM SCENARIOS

To calculate and visualize the internal PIM, n25 DL and n66 DL were considered independently in two potential scenarios because the internal PIM exclusively occurs within the same transmission path.

For the first scenario, the impact of IM3 and IM5 generated by n25 DL signals on the UL frequency was investigated. The PIM calculation involved considering a group of four n25 DL and four n25 UL branches, as the internal PIM only affected the same branches. The center frequency of n25 DL was 1962.5 MHz, whereas that of n25 UL was 1882.5 MHz, serving as inputs for the PIM calculation. Additionally, the total n25 DL and n25 UL bandwidths were used as the inputs. The worst-case scenario occurred when IM3 and IM5 were generated in the same antenna branch because of the total n25 DL bandwidth, resulting in their impact solely on the n25 UL. The ranges of IM3 and IM5, 195 MHz and 325 MHz, respectively, fall within the n25 UL frequency bandwidth.

Fig. 5 provides a visual representation of this scenario. Yellow indicates IM3, spanning a range of 195 MHz, whereas purple represents IM5, spanning a range of 325 MHz. The figure clearly illustrates the impact of n25 DL on n25 UL. Additionally, in FDD, duplex spacing plays a crucial role in determining whether IM products fall within the UL frequency band [25], [68]. Based on Fig. 4, it is suggested that designing a radio with a greater band separation between n25 UL and n25 DL, surpassing the current 15 MHz separation, may mitigate the PIM impact caused by n25 DL. Nevertheless, such an approach involves a trade-off, resulting in reduced bandwidth and spectrum flexibility.

For the second scenario, the impact of IM3 and IM5 generated by n66 DL signals on the UL frequency was analyzed. In this case, a group of four n66 DL branches and four n66 UL branches was considered because the internal PIM only affected the same branches. The center frequencies of the n66 DL and n66 UL were used as inputs, which were 2155 and 1745 MHz, respectively. The total n66 DL and n66 UL bandwidths were also included as inputs. The

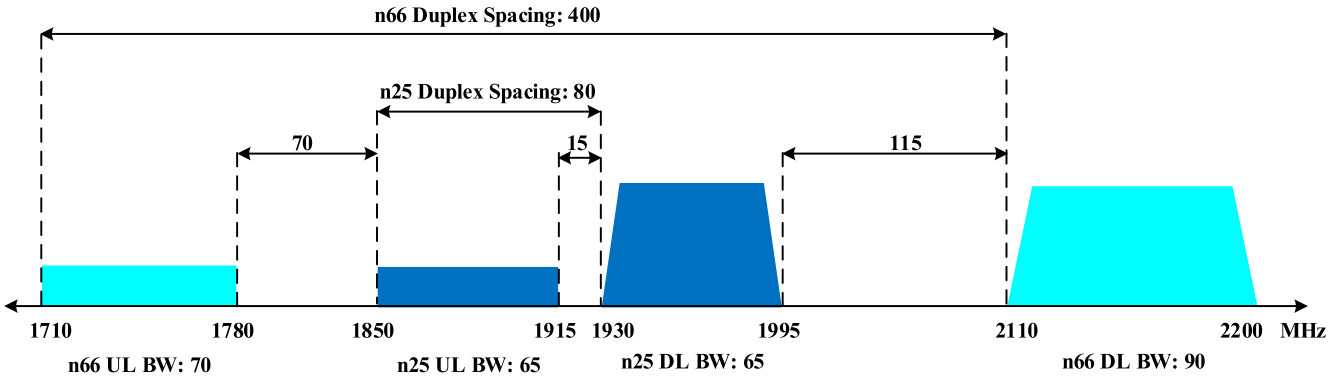

FIGURE 4. Spectrum details for a 5G NR dual band (n25 n66) high-power radio with duplex spacing and band separation.

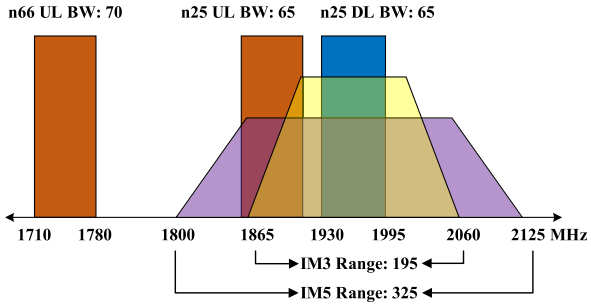

FIGURE 5. Internal PIM, first scenario: IM3 & IM5 generated due to n25 downlink (DL) and its impact on uplink (UL).

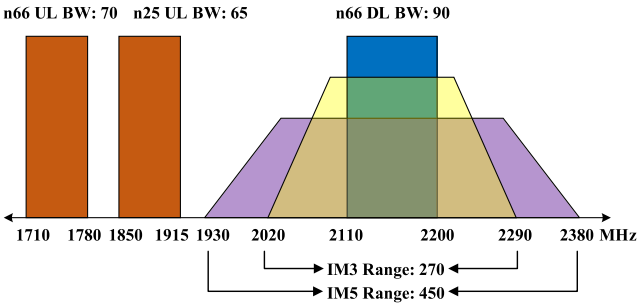

FIGURE 6. Internal PIM, second scenario: IM3 & IM5 generated due to n66 downlink (DL) and its impact on uplink (UL).

ranges of IM3 and IM5 (270 and 450 MHz, respectively) were generated in the same antenna branch because the total n66 DL bandwidth does not affect the n66 UL. Because the PIM generated from the DL frequencies falls outside the RX band, it is classified as an out-of-band PIM and does not impact the UL RX side, as observed in this case.

Fig. 6 provides a visual representation of this scenario. Yellow indicates IM3, spanning a range of 270 MHz, whereas purple represents IM5, spanning a range of 450 MHz. As illustrated in the figure, it is evident that the PIM generated from the n66 DL does not affect the n66 UL.

In summary, the visualizations of PIM interference with an internal PIM source in Fig. 5 and Fig. 6 suggest that PIM is typically not an issue when the duplex spacing is large. However, this example assumes that both bands have an independent RF lineup, and their signals are not mixed within a radio. From a power efficiency perspective, it is often desirable to employ a multi-band PA and combine the bands before the TX PA, assuming the bands fit within the PA operating frequency range. In such a scenario, the signals from the two bands mix within an internal PIM source, creating additional IM products with an overall effect similar to the following external PIM scenario.

B. EXTERNAL PIM SCENARIO

To calculate and visualize the external PIM, both n25 and n66 DL signals were considered because external PIM sources can simultaneously impact all branches.

To calculate the PIM in this scenario, the center frequencies and bandwidths of all the DL and UL bands were utilized as inputs, as mentioned earlier. The worst-case scenario occurs when the frequency ranges of IM3 and IM5, generated by the total n25 DL and n66 DL, affect both n25 UL and n66 UL.

Fig. 7 presents a visual representation of this scenario, assuming the full band conditions. In this scenario, the DL signals from multiple bands and multiple branches mix together in an external PIM source, producing IM3 and IM5 products that affect both n25 and n66 UL. Additionally, the IM5 spans a wide bandwidth and can even extend into the DL band. It is important to note that DL signals from each antenna branch contribute to PIM generation, resulting in multiple PIM hits. For simplicity and ease of visualization, each PIM product is illustrated only once in the figure. Furthermore, PIM interference generated after the duplexer filter (as mentioned in Section V, where the duplexer filter consists of two bandpass filters) and overlapping with the UL band will be preserved by the duplexer RX filter, while the rest of it will be suppressed.

VII. BEHAVIORAL MODELING OF PIM

Various behavioral models are available in the literature to address two types of nonlinear systems: *memoryless nonlinear systems* and *nonlinear systems with memory* [36], [38], [69], [70], [71].

Some well-known memoryless models include the Saleh, Rapp, Fourier series, Bessel-Fourier, Hetrakul and Taylor, and power series models. In contrast, popular models to

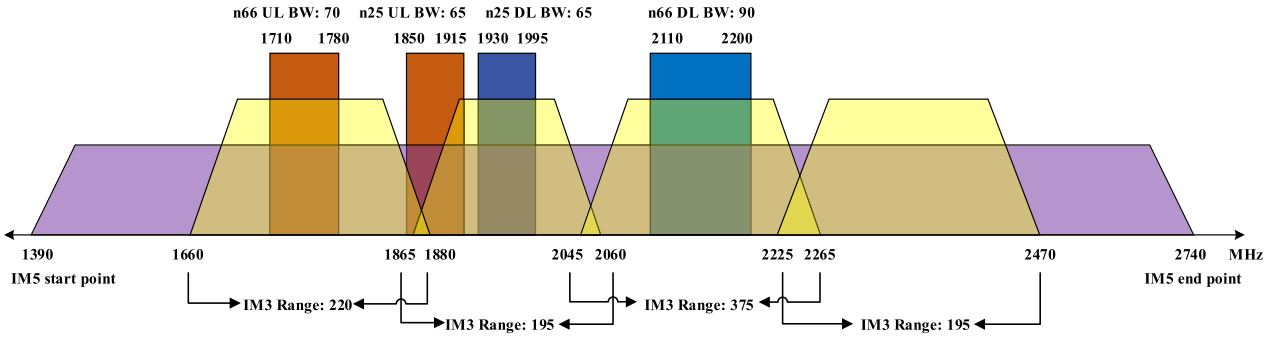

FIGURE 7. External PIM: IM3 & IM5 generated due to n25 and n66 downlink (DL), and its impact on uplink (UL).

address memory impact on nonlinear systems are the Volterra series, memory polynomial (MP), generalized memory polynomial (GMP), and Hammerstein-Wiener models [19], [70]. These models can be applied to understand and employ cancellation techniques for PIM, which is inherently nonlinear. The memory model is particularly realistic and useful in the context of PIM generation, considering the presence of filter units and multi-path effects in the chain.

Specifically, this study focuses on two well-known models, the polynomial power series and Volterra series, to illustrate memoryless nonlinear systems and nonlinear systems with memory.

A. MEMORYLESS NONLINEAR SYSTEMS

A nonlinear system is memoryless if the output at any given time depends only on the input at that time, and not on any previous inputs or outputs. These systems are typically approximated using polynomials [36], [69]. The Power series is helpful for mathematically expressing memoryless nonlinear behavior. It represents a function as an infinite sum of terms, where each term represents a different degree of the input signal. It is a useful tool for approximating many functions as a sum of polynomials, which is easier to calculate than the original function. The input and output of a power series can represent either the voltage, current, or incident and reflected waves in networks [36].

If a nonlinear relationship exists between the current and voltage due to a nonlinear resistor, then the output will have both harmonics and a combination of input signals known as PIM [24], [26], [27]. The nonlinear system's voltage-current relationship can be expressed as i-th order polynomial power series [27], [38], [69], [72], [73]:

$$V = a_0 + a_1 I + a_2 I^2 + a_3 I^3 + \ldots a_i I^i \tag{4}$$

where V is the output voltage, I is the input current of the circuit, and a_0, a_1, a_2, a_3, etc., are coefficients that represent the relationship between the input and output signals. These coefficients represent both the physical properties of nonlinearity and circuit impedances, in which nonlinearity is present [27], [33]. The first term, a_0, represents the DC output or the voltage present at the output when the input current is zero. The second term, $a_1 I$, represents the linear relationship between input and output signals. The third term, $a_2 I^2$, represents the 2nd order nonlinearity, and so on.

First, a single-frequency or single-tone signal is considered as an input signal that is applied to the nonlinear system as

$$I(t) = I_1 \cos(\omega_1 t) \tag{5}$$

where $\omega_1 = 2\pi f_1$, and f_1 is frequency in Hertz.

By substituting (5) into (4), the output voltage of the memoryless nonlinear system up to 3rd order can be expressed as follows:

$$V(t) = a_0 + a_1 I_1 \cos(\omega_1 t) + a_2 I_1^2 \cos^2(\omega_1 t) + a_3 I_1^3 \cos^3(\omega_1 t). \tag{6}$$

Nonlinearity is limited to 3rd order at this point for simplicity. Simplifying (6) using trigonometric relations, the output contains the DC term, the linear term or desired signal, the in-band degradation signal due to 3rd order nonlinearity, the 2nd order harmonics, and the 3rd order harmonics. The DC term, the 2nd order harmonics, and the 3rd order harmonics can be filtered out and do not directly impact the desired signal. Therefore, the output signal is the sum of the desired signal and the in-band degradation signal, which can be expressed as [38] and [36]

$$\hat{V}(t) = a_1 I_1 \cos(\omega_1 t) + \frac{3}{4} a_3 I_1^3 \cos(\omega_1 t). \tag{7}$$

In summary, for a single input frequency, or tone, ω_1, the output will consist of harmonics of the input frequency of the form $n\omega_1$, where $n = 0, 1, 2, \ldots$. These unwanted signals lie outside of the passband and can be filtered.

However, the situation differs for two or more input signals. If the input current I, consisting of two signals I_1 and I_2, also known as two-tone signals, is transmitted through the circuit, it can be expressed as

$$I(t) = I_1 \cos(\omega_1 t) + I_2 \cos(\omega_2 t) \tag{8}$$

where $\omega_i = 2\pi f_i$, and f_i is frequency in Hertz.

By substituting (8) into (4) and simplifying it using trigonometric relations, the resulting output signal can be expressed as (22) in Appendix A. The components of the output signal are listed in Table 3 and can be interpreted as follows [36], [40], [44], [69]:

TABLE 3. Components of output signal due to 3rd order nonlinearity when the input signal is two-tone.

No.	Frequency	Amplitude
1	DC	$a_0 + \frac{1}{2}a_2(I_1^2 + I_2^2)$
2	ω_1	$a_1 I_1 + \frac{3}{2}a_3(\frac{1}{2}I_1^3 + I_1 I_2^2)$
3	ω_2	$a_1 I_2 + \frac{3}{2}a_3(\frac{1}{2}I_2^3 + I_1^2 I_2)$
4	$2\omega_{i=1,2}$	$\frac{1}{2}a_2 I_i^2$ for i = 1,2
5	$3\omega_{i=1,2}$	$\frac{1}{4}a_3 I_i^2$ for i = 1,2
6	$(\omega_1 \pm \omega_2)$	$a_2 I_1 I_2$
7	$(2\omega_1 \pm \omega_2)$	$\frac{3}{4}a_3 I_1^2 I_2$
8	$(2\omega_2 \pm \omega_1)$	$\frac{3}{4}a_3 I_1 I_2^2$

1. The DC components represent the average value of the PIM signal.

2 & 3. The components are proportional to the input signal, which is a useful signal because the output is proportional to the product of the input currents and the degradation term due to 3rd order nonlinearity.

4 & 5. The 2nd and 3rd order harmonics terms are not considered harmful because they are far from the useful signals and can be removed by filtering.

6. Components with the sum and difference of the input frequencies also fall outside the band and can be removed by filtering.

7 & 8. The PIM products into their constituent frequencies, which are the harmonics of the input frequencies. For example, the term $(2\omega_1 - \omega_2)$ represents a frequency component that is twice the frequency of ω_1 and once the frequency of ω_2. The sum and differences are represented by $(2\omega_1 \pm \omega_2)$ and $(2\omega_2 \pm \omega_1)$ which are known as IM3.

Furthermore, it is possible to calculate the power from the amplitudes listed in Table 3 because the power of a signal is directly proportional to the square of its amplitude. For IM3 with frequency $(2\omega_1 - \omega_2)$, the power can be derived as [27] and [39]

$$P_{IM3} \propto (\frac{3}{4}a_3 I_1^2 I_2)^2 \approx (I_1^2 I_2)^2 \approx P_1^2 P_2 \tag{9}$$

where P_1 and P_2 are the powers of the fundamental signals, and P_{IM3} is the power of the IM3 responses.

From (9), if the power series is limited to the 3rd order nonlinearities then only IM3 products with a "1 dB-3 dB" power relation are produced, given that both P_1 and P_2 are increased by 1 dB. In other words, each 1 dB increase in the carrier power leads to a 3 dB increase in the IM3 power. However, if either P_2 or P_1 remains constant while the other changes, the slopes are 2 dB per dB and 1 dB per dB, respectively [27], [39].

The 5th, 7th, and 9th order terms also generate IM3 frequencies. It has been mathematically proven that higher-order terms are products of two lower-order terms [27], [74]. The 5th order nonlinearity produces both IM3 and IM5, as shown in Appendix B. In this case, when $(a_1, a_5 \neq 0\, a_3 = 0)$, both IM3 and IM5 follow a "1 dB-5 dB" relation. Furthermore, at small signal levels, a higher-order coefficient a_5 can be ignored, and consider only $a_3 \neq 0$. Subsequently, the IM power at frequency $(2\omega_1 - \omega_2)$ increases by 2 dB per dB with signal amplitude I_1 and by 1 dB per dB with signal amplitude I_2. However, this simplification is not valid for high-power signal levels. Therefore, a_5 and higher coefficients are non-zero, and the relation between the signal and IM is complex and depends on all the coefficients in the power series [27].

In addition, from Table 3, the generalization of the output spectrum can be derived in the form $|\pm nf_1 \pm mf_2|$ where $|n + m|$ represents the order of the PIM signals [24], [26], [36], [38], [39].

The power series model assumes that the system's response to an input signal is only a function of the input signal without any memory impact. It can be used to analyze nonlinear systems, whose output strictly depends on the input signal at a particular time. However, this assumption is not always valid. A major drawback of power series-based PIM analysis is its inability to model the memory effects in a circuit [36]. As communication signals become wider in modern wireless communication systems, the need for advanced models that can describe nonlinear memory effects has become evident [70]. In particular, when the frequency band exceeds 10 MHz, it is essential to consider the impact of memory [69].

B. NONLINEAR SYSTEMS WITH MEMORY

If a system depends on its present and past inputs, it is referred to as a system with memory. Such systems can store energy through reactive elements [69]. To analyze the output of a nonlinear system with memory impact, the Volterra series can be employed to study the IM properties of time-varying circuits [36]. It is a widely used mathematical tool for modeling nonlinear functions including memory [70].

Consider a linear, causal, and time-invariant system with memory characterized by an input signal $x(t)$, an impulse response $h(t)$, and an output signal $y(t)$. This system can be mathematically represented using a convolution integral as [36], [75], and [76]

$$y(t) = \int_{-\infty}^{+\infty} h(\tau)x(t-\tau)d\tau. \tag{10}$$

The Volterra series combines (10) and (1) to describe a nonlinear system with memory [36], [75], [77], [78]. For each order n in the expansion, the series provides a corresponding impulse response known as the Volterra kernel h_n. The system output is obtained by performing an n-th order convolution integral between the delayed input signal and Volterra kernel. This operation can be expressed as [35], [36], [37], [75], [77], and [79]

$$y(t) = H_1[x(t)] + H_2[x(t)] + H_3[x(t)] + \ldots H_n[x(t)] \tag{11}$$

in which

$$H_n[x(t)] = \int_{-\infty}^{+\infty} \ldots \int_{-\infty}^{+\infty} h_n(\tau_1, \tau_2, \ldots, \tau_n) \times x(t-\tau_1)x(t-\tau_2)\ldots x(t-\tau_n)d\tau_1 d\tau_2 \ldots d\tau_n. \tag{12}$$

Hence, the Volterra series is an infinite sum of n-fold convolution integrals [36], [75]. Here, $H_n[.]$ is the n-th order Volterra operator, and $h_n(\tau_1, \tau_2, \ldots, \tau_n)$ is the n-th order Volterra kernel.

Furthermore, frequency domain Volterra kernels are required to calculate harmonics and IM products. Therefore, from the time domain to the frequency domain, Volterra kernels via Fourier transform can be expressed as [36], [75], and [79]

$$\begin{aligned} &H_n(j\omega_1, \ldots, j\omega_n) \\ &= F[h_n(\tau_1, \tau_2, \ldots, \tau_n)] \\ &= \int_{-\infty}^{+\infty} \ldots \int_{-\infty}^{+\infty} h_n(\tau_1, \ldots, \tau_n) e^{-j\omega_1 \tau_1} \\ &\quad \ldots e^{-j\omega_n \tau_n} d\tau_1 \ldots d\tau_n \end{aligned} \tag{13}$$

where H_n is the frequency domain of the Volterra kernel. Finally, the output of the n-th order nonlinear system with memory impact in the frequency domain can be formulated as [75]

$$\begin{aligned} Y = &H_1(j\omega_{p1}) \circ I + H_2(j\omega_{p1}, j\omega_{p2}) \circ I^2 \\ &+ \ldots + H_n(j\omega_{p1}, j\omega_{p2}, \ldots j\omega_{pn}) \circ I^n \end{aligned} \tag{14}$$

where I is the input of m frequency components, and $j\omega_{p1}, j\omega_{p2}, \ldots j\omega_{pn}$ can be chosen from all possible n out of m permutations of $\pm\omega_1, \pm\omega_2, \ldots, \pm\omega_m$. For each term, the frequency components in H_n are the same as those in I^n.

For two-tone signals, by substituting (8) into (14), it is possible to calculate IM3, IM5, and so on.

The Volterra model is accurate but complex. In practice, systems that employ memory models are constructed based on the most essential terms within the Volterra series. These are referred to as reduced Volterra series models or pruned-Volterra series models. MP and GMP serve as prime examples of reduced Volterra series models and find widespread utilization [19], [70]. Recent studies have applied these two models to digital PIM cancellation techniques [56], [65], [67].

To measure and compare the complexity among behavioral models, the number of parameters used in the model is a yardstick that determines the memory size required for a behavioral model. However, this method is not always accurate. Another popular method used to measure complexity is the number of floating-point operations or FLOPs, which is sufficiently accurate to make fair comparisons between behavioral models. In terms of model performance, the Normalized Mean Square Error (NMSE) is commonly used [70], [71].

In summary, it is possible to model PIM for memoryless nonlinear systems and systems with memory. The derived equations represent PIM products that can be generated by nonlinearities in the passive components of a wireless communication system. These PIM products can interfere with desired signals and degrade the overall performance of the system. Therefore, it is important to design and implement digital PIM cancellation techniques to minimize PIM products in multi-band high-power MIMO FDD radios.

VIII. PIM MITIGATION APPROACHES

When it comes to PIM interference minimization and mitigation approaches, a straightforward solution is to lower the transmission power, as this can substantially reduce or completely eliminate the PIM. Alternatively, RX sensitivity requirements can be relaxed to allow a certain level of desensitization. These approaches are commonly referred to as maximum power reduction (MPR) and maximum sensitivity degradation (MSD), respectively. However, their immediate consequences are cell coverage, power efficiency, and throughput reduction; therefore, they are not the preferred choices. PIM can also be avoided through proper radio resource management, that is, smart UL and DL resource allocation, such that a power limited UL user at a cell edge is prioritized for scheduling in a frequency bin that does not overlap with PIM interference. However, this approach limits spectrum utilization, and consequently, peak data rates. Lastly, improving the quality and isolation of RF components can also reduce PIM, but this can, unfortunately, substantially increase the transceiver implementation cost [9], [22], [59], [80], [81], [82], [83], [84], [85], [86], [87], [88].

Over the past half-century, research has primarily focused on phenomena, measurements, and mechanisms related to PIM [26], [47]. Earlier studies proposed several hardware-dependent PIM cancellation techniques. For instance, Henrie et al. [83] presented a technique that enhances PIM cancellation by controlling the thickness of nickel and gold plating on the conductors of a coaxial transmission line. Jin et al. [89] theoretically modeled and analyzed the effect of ferromagnetic characteristics in coating materials and base copper alloys on the PIM performance. Wang et al. [90] investigated the PIM behavior of TNC coaxial connectors while considering the temperature changes. Jung et al. [91], [92] proposed band separation and frequency planning to suppress IM3 by 4-5 dB, which proved effective in narrow-channel bandwidth systems, such as 2G. However, these approaches are not effective in suppressing PIM in wide-channel bandwidth systems (LTE, NR) and/or when CA is activated or multiple frequency bands are involved [91]. Another PIM cancellation technique based on an adaptive filter algorithm was proposed; however it requires complex analog circuitry to generate a reference signal for the adaptive algorithm [93].

A. DIGITAL PIM CANCELLATION TECHNIQUES

In general, the physical techniques described above cannot fully mitigate the PIM interference, and they have an associated high cost for hardware implementation. As a result, there is a growing interest in digital PIM mitigation techniques in which the cancellation solution can dynamically model and cancel the time-varying PIM. Digital cancellation techniques operate in the baseband and thus offer a simplified and flexible solution for transceiver implementation.

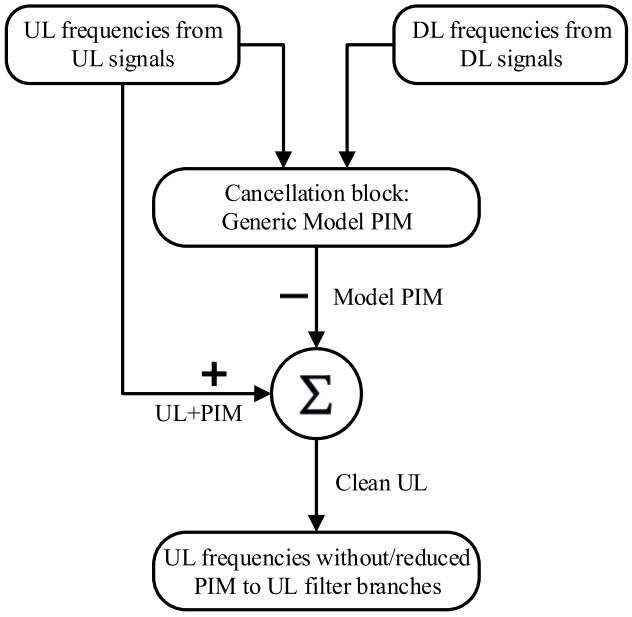

FIGURE 8. Block diagram of PIM cancellation technique.

The fundamental idea behind digital PIM cancellation is based on the adaptive filtering principle, where it is assumed that the PIM-induced interference in the RX is a nonlinear function of the original transmit signal. Therefore, a parametric model can be employed to estimate the PIM coupling channel response. For the algorithm, both sample-adaptive or block-adaptive estimation algorithms can be utilized. Finally, with the estimated parameters and known transmit signal, a replica of the PIM interference can be generated within the transceiver, which is then subtracted from the received signal to reduce the effects of PIM interference in the UL. A conceptual illustration of the digital PIM cancellation solution is presented in Fig. 8.

B. EXAMPLES OF DIGITAL PIM CANCELLATION

Among the digital PIM mitigation techniques reported in the recent literature, Tian et al. [74], [94] proposed a method for suppressing PIM in digital satellite communications. However, it is difficult to implement this solution in practice because of the time delay, frequency offset, and phase offset between the received and estimated PIM signals.

Kearney et al. [33] presented a technique for single-band PIM cancellation that models PIM based on transmitting and receiving signals. However, this technique has limitations in multi-band scenarios.

The intermodulated part impacting the received signal can be measured and subsequently suppressed due to its high correlation with the transmitted signal. This method was implemented to cancel the IM2 [42], [57]. Kamizuma et al. [95] proposed a technique to cancel IM3 in an LTE BS by regenerating IM3 from IM2. However, this technique does not address higher-order PIM products.

A new method, the dynamic cancellation of higher-order PIM interference, which is practically possible to implement in the radio, was illustrated in [91]. PIM interference is estimated dynamically from the transmitted signal in the form of coefficients. The PIM interference is cancelled out from the RX path. Dynamic PIM interference estimation comes from as a function of the transmitted signal, and the function includes coefficient(s), which model the properties of the radio to measure PIM interference. A test signal is transmitted to gauge the coefficient when the radio is not scheduled to receive any signal. Then, during transmission, the radio takes advantage of the coefficient(s) to dynamically estimate and cancel PIM interference. For the test signal, a time slot must be reserved that could interfere with ongoing communication.

Furthermore, several studies have described external PIM cancellation techniques based on the basis function method and channel coefficient method in a dual-band rank-2 MIMO system with CA [56], [65], [67]. However, with an increase in IM order, the number of basis functions increased significantly, resulting in higher complexity. For IM3, it ranged from 6 to 8, and for IM5, it ranged from 34 to 48. In addition, the basis function method overlooked memory effects, whereas the channel coefficient method approximated the channel between the transceiver and an external PIM source using a single tap [56].

In a recent study on digital PIM cancellation, the modeling and cancellation of external PIM in 5G NR band n3 MIMO FDD transceivers based on a Wiener-Hammerstein model was presented by Lampu et al. [22]. A general solution for any number of parallel transceiver chains was described. To reduce the complexity of the cancellation engine, a spline-interpolated lookup table and least mean squares-based parameter adaptation were utilized. The results were compared for IM5 with the authors' previous work in [56] for two CCs (5 MHz and 20 MHz each). For the case of 5 MHz CCs, the cancellation was achieved 18.3 dB versus around 17.5 dB of their previous work. However, for 20 MHz CCs, the cancellation was achieved around 14.7 dB for both cases.

Machine learning techniques have also been discussed in some studies to mitigate PIM. Tsui et al. [66] proposed a PIM cancellation system that generates an error signal, and utilized it to train a learning system for interference cancellation. However, the implementation of this method requires network downtime during the maintenance window, which poses a practical limitation. Jang et al. [96], [97] described a Focused Time Delay Neural Network for modeling IM3, but its applicability is limited to addressing IM3 exclusively. Additionally, Mismar proposed a supervised approach using linear regression to detect IM interference without the need to inject test tones or channel noise [68]. However, linear regression is unsuitable to address nonlinear phenomena. It is important to note that accurate modeling of interference in large network scenarios requires training and testing data, which may present a potential drawback for this case.

A straightforward method for canceling the IM3 with memory characteristics using the Volterra series in two

TABLE 4. PIM mitigation techniques, and their performance.

PIM Mitigation Techniques	Literature	Point of Cancellation	Degree of Cancellation	Cancellation Performance	Dependency	Complexity
Prevention Techniques	Henrie *et al.* [83] ; Jin *et al.* [89] ; Wang *et al.* [90];	conductors, ferromagnetic materials, coaxial connectors	-	-	Hardware	High
RF Cancellation	Jung *et al.* [92]; Keehr *et al.* [93]	RF, Baseband	IM3	24 dB	Hardware	High
Digital Cancellation	Tian *et al.* [74], [94]; Kearney *et al.* [33]; Kamizuma *et al.* [95]; Wang *et al.* [91]; Lampu *et al.* [22], [56], [65], [67]; Waheed *et al.* [81]	Baseband	IM2, IM3, IM5, IM9	11-19.6 dB	Software	Low

different bands was proposed in [96], [98]. This method can be extended to cancel the higher-order IM products.

Table 4 summarizes all the major PIM mitigation techniques and categorizes them into three groups: prevention techniques, RF cancellation, and digital cancellation.

C. PIM MODELING FOR DIGITAL CANCELLATION

To demonstrate the digital PIM cancellation approach, consider the baseband complex representations of the transmitted signals f_1 and f_2 as $x_1(n)$, and $x_2(n)$, respectively. The received baseband UL signal $y(n)$ with center frequency $f_{RX} = 2f_1 - f_2$ is given by [74], [96], [98]

$$y(n) = r(n) + p(n) + v(n) \tag{15}$$

where $r(n)$, $p(n)$, and $v(n)$ represent the UL signal, PIM, and additive white Gaussian noise, respectively.

A memory length of M is considered, and the nonlinear relationship between $p(n)$ and the DL signals ($x_1(n)$ and $x_2(n)$) is described by the function $H[.]$. This relationship can be expressed as [96] and [98]

$$p(n) = H[x_1(n), \ldots, x_1(n-M+1), x_2(n), \ldots, x_2(n-M+1)]. \tag{16}$$

The proposed cancellation model is [74], [80], [98]

$$\hat{r}(n) = y(n) - \hat{p}(n) = r(n) + p(n) + v(n) - \hat{p}(n) \approx r(n) + v(n) \tag{17}$$

where $\hat{r}(n)$ and $\hat{p}(n)$ represent the estimated UL signal and model PIM output, respectively, described in (16).

The modified cubic Volterra filter (CVF) [99] was implemented to model the PIM $p(n)$ with the two DL signals f_1, and f_2. The PIM located at the center frequency $f_{RX} = 2f_1 - f_2$ is generated from passband signals with two different frequencies, which are complex conjugates of x_1, and x_2 [37]. When a two-tone 3rd order polynomial with a memory length of M-1 is considered, the model PIM $\hat{p}(n)$ can be expressed as [96] and [98]

$$\hat{p}(n) = \sum_{k_1=0}^{M-1}\sum_{k_2=0}^{M-1}\sum_{k_3=0}^{M-1} h_c^F(k_1,k_2,k_3) \times x_1(n-k_1)x_1(n-k_2)x_2^*(n-k_3) \tag{18}$$

where $h_c^F(k_1,k_2,k_3)$ represent the filter coefficients and the superscript * denotes the conjugate. Considering the symmetry $x_1(n-k_1)x_1(n-k_2) = x_1(n-k_2)x_1(n-k_1)$ in (18), it can be reduced to [96], [98]

$$\hat{p}(n) = \sum_{k_1=0}^{M-1}\sum_{k_2=k_1}^{M-1}\sum_{k_3=0}^{M-1} h_c(k_1,k_2,k_3) \times x_1(n-k_1)x_1(n-k_2)x_2^*(n-k_3) \tag{19}$$

where $h_c(k_1,k_2,k_3)$ represent the corresponding CVF coefficients for the reduced input components and the time index k_2 starts from k_1. The number of coefficients $h_c^F(k_1,k_2,k_3)$ is $N = M^2(M+1)/2$ in (19) and M^3 in (18).

In vector form, (18) can be expressed as [96] and [98]

$$\hat{p}(n) = h_c x_c(n) \tag{20}$$

where the coefficient vector h_c is a $1 \times N$ row vector consisting of the coefficients $h_c(k_1,k_2,k_3)$ with $N = M^2(M+1)/2$ and the input vector $x_c(n)$ is an $N \times 1$ column vector consisting $x_1(n-k_1)x_1(n-k_2)x_2^*(n-k_3)$.

When the Wiener-Hopf equation [100] is used to estimate the coefficient vector h_c, (20) can be expressed for K samples of the signal $\hat{p}(n)$ as [96] and [98]

$$\hat{p} = h_c X_c \tag{21}$$

where $\hat{p}$ is a $1 \times K$ row vector with $\hat{p}(n)$ and X_c is an $N \times K$ vector with $X_c(n)$, $n = 0, 1, \ldots, K-1$. Finally, the estimated model vector of the PIM is subtracted from the received signal.

Table 5 summarizes the algorithms and performance of the major digital PIM cancellation techniques proposed in recent literature considering memory impact. Note that the computational cost of eliminating all PIM orders can be high;

TABLE 5. Algorithm and performance comparison in the major literature for effective digital PIM cancellation techniques in radio systems, considering the memory impact of external PIM sources.

Literature	Algorithm	Cancellation	Signal/TX (MHz)	PIM Terms	Complexity (FLOPs)	Cancellation Performance
Lampu *et al.* [22]	Wiener-Hammerstein	IM5	two CCs, 5	Cascaded	196	18.3 dB
Lampu *et al.* [56]	GMP	IM5 & IM9	two CCs, 5	760 & 65-100	3340	17.3-19.6 dB
Waheed *et al.* [81]	MP	IM3	two CCs, 2.5	42	Low	21 dB
Kamizuma *et al.* [95]	Feed-forward	IM3	5	-	Low	11-13 dB
Jang *et al.* [98]	Volterra	IM3	5	6	Low	2.267×10^{-4} NMSE

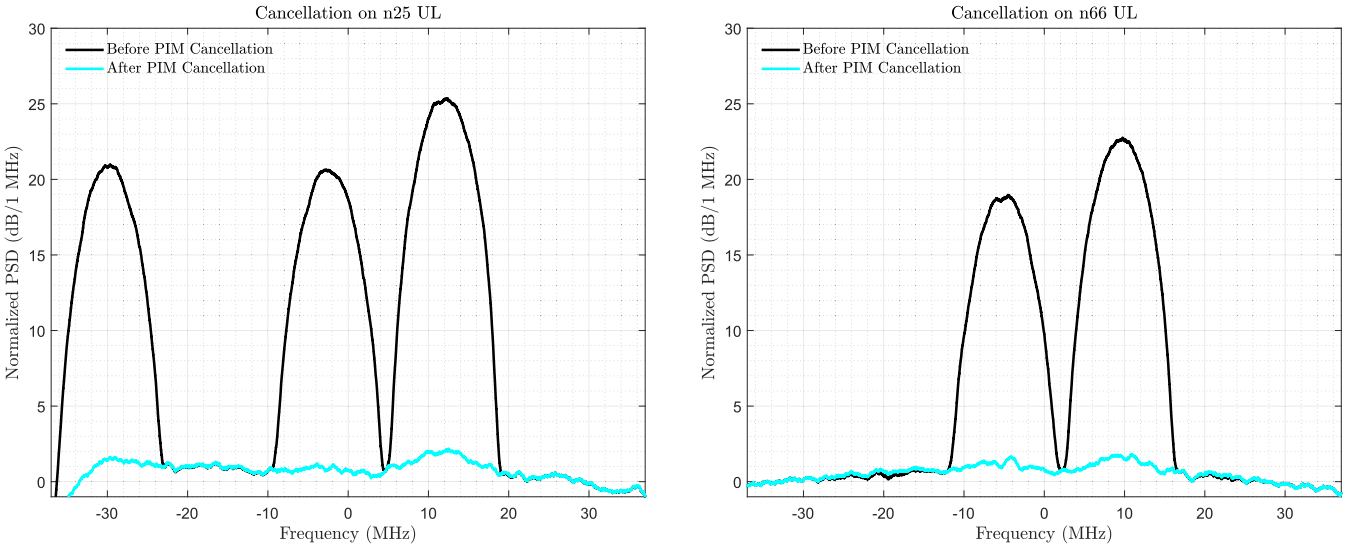

FIGURE 9. Power Spectral Density (PSD) curves of PIM interference before and after digital cancellation in n25 and n66 UL, when there are two downlink carriers allocated in each band. The bandwidth of each carrier is 5MHz and PIM source is external.

therefore, it is often more practical to focus on only the first few orders (e.g., 3rd, 5th, and 7th) to achieve acceptable performance.

IX. MEASUREMENT EXAMPLES OF DIGITAL PIM CANCELLATION

In this section, we demonstrate the potential of digital PIM cancellation through true RF measurements carried out using commercial dual-band n25 and n66 radio unit. For simplicity, the measurement example assumes a single TX and RX operation per band with an external PIM object, where DL signals from both bands are mixed together. The total TX power was +46 dBm, and the PIM source was located approximately 1m from the antenna. The resulting PIM interference is observed in the UL of both bands, consistent with the discussion in Section VI-B (Fig. 7). However, as opposed to full-band allocation, we consider two different scenarios with different numbers of carrier combinations. The digital cancellation technique adopted for PIM suppression is based on the principle described in Section VIII.

In the first scenario, we allocate two non-contiguously aggregated NR-5 MHz carriers per band. For n25, the RF center frequencies of the carriers are set at 1932.5 MHz and 1987.5 MHz, and for n66, they are placed at 2125 MHz and 2165.5 MHz, respectively. The observed PIM before and after digital cancellation is plotted in Fig. 9, revealing three PIM hits in the n25 UL and two PIM hits in the n66 UL. Notably, the strength of the PIM interference relative to the system noise floor is substantial, reaching up to 25 dB. The digital cancellation technique effectively mitigates interference close to the noise floor.

In the second scenario, an additional carrier is now added to each band, resulting in three carriers per band. The RF center frequencies of the carriers are now 1932.5 MHz, 1976 MHz, and 1987.5 MHz for n25, and 2135 MHz, 2150 MHz, and 2176 MHz for n66, respectively. In line

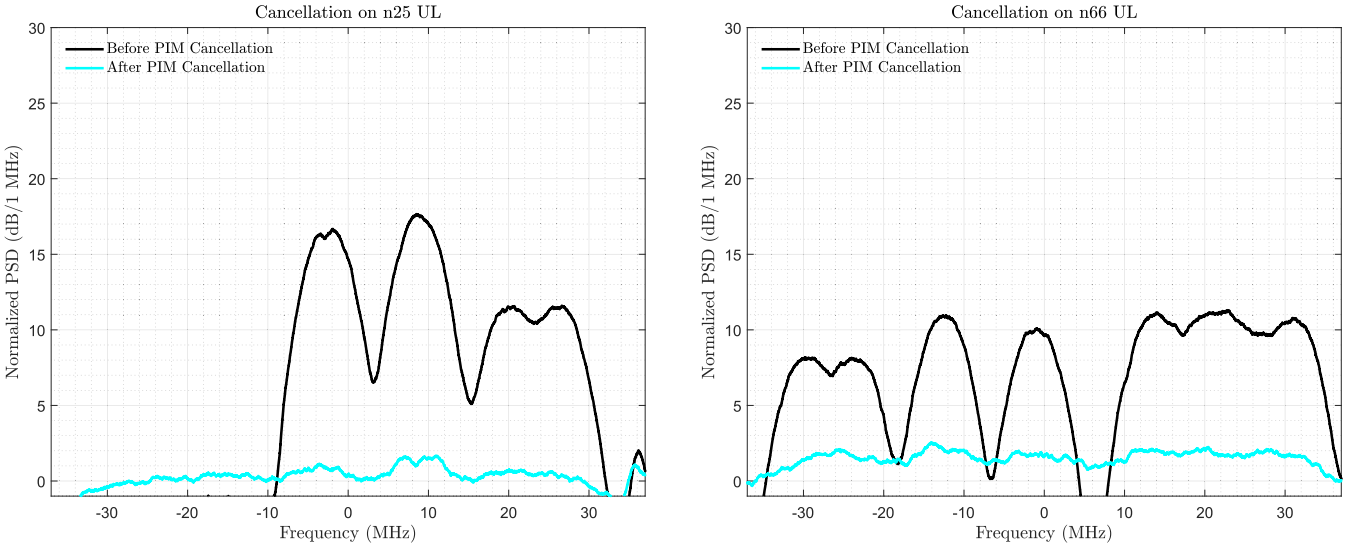

FIGURE 10. Power Spectral Density (PSD) curves of PIM interference before and after digital cancellation in n25 and n66 UL, when there are three downlink carriers allocated in each band. The bandwidth of each carrier is 5MHz and PIM source is external.

with our discussion in Section V, where we explained that more carriers give rise to more PIM products, the observed PIM shown in Fig. 10 now spans a much wider bandwidth and completely overlaps with the n66 band. However, the relative strength of the PIM interference is reduced compared to Fig. 9 because the PIM power is now spread over a larger bandwidth. Nevertheless, the digital cancellation technique can effectively suppress interference close to the noise floor.

Finally, it is worth mentioning that while the digital cancellation technique offers a flexible solution to mitigate PIM, its complexity typically increases as the number of *aggressor carriers* increases. Ongoing research is focused on advanced signal modeling and estimation techniques aimed at reducing the implementation complexity of digital cancellation solutions.

X. CONCLUSION AND LESSONS LEARNED

Passive nonlinearities in components introduce unwanted IM in the BS, which can potentially degrade the performance of wireless networks and may even cause communication disruptions. Therefore, the mitigation of PIM is crucial for modern wireless communication systems. This paper presents a detailed analysis of the PIM with an example of a dual-band high-power MIMO FDD radio and highlights its impact on radio performance. Moreover, this paper discusses theoretical models and practical digital cancellation techniques that can be employed to mitigate PIM in real networks. This study sheds light on the significance of PIM cancellation and provides insights into state-of-the-art techniques to mitigate this unwanted phenomenon in wireless networks.

As a final remark, PIM has been a persistent challenge in wireless telecommunication networks, and it will continue to be so in the future. As the demand for higher data rates and spectrum allocation at higher frequencies increases, the need for more BS increases. Consequently, PIM remains a significant challenge and innovative PIM mitigation solutions, including digital cancellation techniques, will remain a critical topic for research and development in the coming decades.

APPENDIX A
FINAL OUTCOME OF 3RD ORDER POLYNOMIAL FOR MEMORYLESS SYSTEMS

This appendix presents the final outcome of 3rd order polynomial for memoryless systems using a power series.

$$\begin{aligned} V(t) = a_0 &+ \frac{a_2}{2}(I_1^2 + I_2^2) + a_1(I_1\cos(\omega_1 t) + I_2\cos(\omega_2 t)) \\ &+ \cos(\omega_1 t)\left(\frac{3a_3 I_1^3}{4} + \frac{3a_3 I_1 I_2^2}{2}\right) \\ &+ \cos(\omega_2 t)\left(\frac{3a_3 I_2^3}{4} + \frac{3a_3 I_1^2 I_2}{2}\right) + \cos(2\omega_1 t)\left(\frac{a_2 I_1^2}{2}\right) \\ &+ \cos(2\omega_2 t)\left(\frac{a_2 I_2^2}{2}\right) + \cos(3\omega_1 t)\left(\frac{a_3 I_3^3}{4}\right) \\ &+ \cos(3\omega_2 t)\left(\frac{a_3 I_2^3}{4}\right) + \cos((\omega_1 \pm \omega_2)t)(a_2 I_1 I_2) \\ &+ \cos((2\omega_1 \pm \omega_2)t)\left(\frac{3a_3 I_1^2 I_2}{4}\right) \\ &+ \cos((2\omega_2 \pm \omega_1)t)\left(\frac{3a_3 I_1 I_2^2}{4}\right) \end{aligned} \tag{22}$$

APPENDIX B
HIGHER-ORDER PIM PRODUCING LOWER-ORDER PIM

Theoretically, higher-order PIM include lower-order ones. For instance, 5th order PIM includes both 3rd and 5th order IM coefficients, as shown in (23) [27], [74]:

$$\begin{aligned} &a_5[I_1\cos(\omega_1 t) + I_2\cos(\omega_2 t)]^5 \\ &= a_5[I_1\cos(\omega_1 t) \\ &\quad + I_2\cos(\omega_2 t)]^2[I_1\cos(\omega_1 t) + I_2\cos(\omega_2 t)]^3 \end{aligned}$$

$$= [a_3\frac{3I_1^2I_2}{4} + a_5[(\frac{I_1^2}{2}+\frac{I_2^2}{2})\frac{3I_1^2I_2}{4} + \frac{I_1^2}{4}\frac{3I_1I_2^2}{4} + \frac{I_2^2}{4}\frac{3I_1^2I_2}{4} + \frac{3I_1^2I_2}{4}(\frac{I_1^2}{2}+I_2^2+\frac{I_1^3}{4})]]\cos((2\omega_1-\omega_2)t). \quad (23)$$

REFERENCES

[1] E. Dahlman, S. Parkvall, and J. Skold, *5G NR: The Next Generation Wireless Access Technology*, 2nd ed. Amsterdam, The Netherlands: Elsevier, 2020.

[2] *NR; Base Station (BS) Radio Transmission and Reception (Release 18)*, document TS 38.101-3, v18.1.0, 3GPP, Mar. 2023.

[3] *NR; NR and NG-RAN Overall Description; Stage 2 (Release 17)*, document TS 38.300, V17.4.0, 3GPP, Mar. 2023.

[4] H. Ji, Y. Kim, J. Lee, E. Onggosanusi, Y. Nam, J. Zhang, B. Lee, and B. Shim, "Overview of full-dimension MIMO in LTE-advanced pro," *IEEE Commun. Mag.*, vol. 55, no. 2, pp. 176–184, Feb. 2017.

[5] P. Merias. (Aug. 8, 2022). *Carrier Aggregation on Mobile Networks*. Accessed: Oct. 23, 2023. [Online]. Available: https://www.3gpp.org/technologies/carrier-aggregation-on-mobile-networks

[6] *LTE Time Division Duplex (TDD)—Frequency Division Duplex (FDD) Joint Operation Including Carrier Aggregation (CA) (Release 12)*, document TS 36.847, V12.0.0, 3GPP, Dec. 2013.

[7] *Release 16 Description; Summary of Rel-16 Work Items (Release 16)*, document TS 21.916, V16.2.0, 3GPP, Jun. 2022.

[8] W. Chen, X. Lin, J. Lee, A. Toskala, S. Sun, C. F. Chiasserini, and L. Liu, "5G-advanced toward 6G: Past, present, and future," *IEEE J. Sel. Areas Commun.*, vol. 41, no. 6, pp. 1592–1619, Jun. 2023.

[9] *NR; User Equipment (UE) Radio Transmission and Reception; Part 3: Range 1 and Range 2 Interworking Operation With Other Radios (Release 18)*, document TS 38.101-3, V18.1.0, 3GPP, Mar. 2023.

[10] W. Chen, P. Gaal, J. Montojo, and H. Zisimopoulos, *Fundamentals of 5G Communications: Connectivity for Enhanced Mobile Broadband and Beyond*. New York, NY, USA: McGraw-Hill, 2021.

[11] X. Lin, J. Li, R. Baldemair, J. T. Cheng, S. Parkvall, D. C. Larsson, H. Koorapaty, M. Frenne, S. Falahati, A. Grovlen, and K. Werner, "5G new radio: Unveiling the essentials of the next generation wireless access technology," *IEEE Commun. Standards Mag.*, vol. 3, no. 3, pp. 30–37, Sep. 2019.

[12] H. Holma, A. Toskala, and T. Nakamura, *5G Technology: 3GPP New Radio*. Hoboken, NJ, USA: Wiley, 2020.

[13] T. S. Rappaport, Y. Xing, O. Kanhere, S. Ju, A. Madanayake, S. Mandal, A. Alkhateeb, and G. C. Trichopoulos, "Wireless communications and applications above 100 GHz: Opportunities and challenges for 6G and beyond," *IEEE Access*, vol. 7, pp. 78729–78757, 2019.

[14] N. Rajatheva, I. Atzeni, S. Bicaïs, E. Björnson, A. Bourdoux, S. Buzzi, C. D'andrea, J.-B. Doré, S. Erkucuk, M. Fuentes, and K. E. Guan, "Scoring the terabit/s goal: Broadband connectivity in 6G," 2020, *arXiv:2008.07220*.

[15] H. Tataria, M. Shafi, A. F. Molisch, M. Dohler, H. Sjöland, and F. Tufvesson, "6G wireless systems: Vision, requirements, challenges, insights, and opportunities," *Proc. IEEE*, vol. 109, no. 7, pp. 1166–1199, Jul. 2021.

[16] D. Serghiou, M. Khalily, T. W. C. Brown, and R. Tafazolli, "Terahertz channel propagation phenomena, measurement techniques and modeling for 6G wireless communication applications: A survey, open challenges and future research directions," *IEEE Commun. Surveys Tuts.*, vol. 24, no. 4, pp. 1957–1996, 4th Quart., 2022.

[17] X. Lin, "An overview of the 3GPP study on artificial intelligence for 5G new radio," 2023, *arXiv:2308.05315*.

[18] X. Lin, L. Kundu, C. Dick, and S. Velayutham, "Embracing AI in 5G-advanced towards 6G: A joint 3GPP and O-RAN perspective," 2022, *arXiv:2209.04987*.

[19] D. R. Morgan, Z. Ma, J. Kim, M. G. Zierdt, and J. Pastalan, "A generalized memory polynomial model for digital predistortion of RF power amplifiers," *IEEE Trans. Signal Process.*, vol. 54, no. 10, pp. 3852–3860, Oct. 2006.

[20] A. Kiayani, M. Abdelaziz, L. Anttila, V. Lehtinen, and M. Valkama, "Digital mitigation of transmitter-induced receiver desensitization in carrier aggregation FDD transceivers," *IEEE Trans. Microw. Theory Techn.*, vol. 63, no. 11, pp. 3608–3623, Nov. 2015.

[21] J. Jokinen, "Passive intermodulation in high-power radio transceivers," M.S. thesis, Tampere Univ. Technol., 2016.

[22] V. Lampu, L. Anttila, M. Turunen, M. Fleischer, J. Hellmann, and M. Valkama, "Cancellation of air-induced passive intermodulation in FDD MIMO systems: Low-complexity cascade model and measurements," in *IEEE MTT-S Int. Microw. Symp. Dig.*, Jun. 2023, pp. 33–36.

[23] A. Kiayani, V. Lehtinen, L. Anttila, T. Lahteensuo, and M. Valkama, "Linearity challenges of LTE-advanced mobile transmitters: Requirements and potential solutions," *IEEE Commun. Mag.*, vol. 55, no. 6, pp. 170–179, Jun. 2017.

[24] Z. Cai, L. Liu, F. de Paulis, and Y. Qi, "Passive intermodulation measurement: Challenges and solutions," *Engineering*, vol. 14, pp. 181–191, Jul. 2022.

[25] C. Motz, T. Paireder, H. Pretl, and M. Huemer, "A survey on self-interference cancellation in mobile LTE-A/5G FDD transceivers," *IEEE Trans. Circuits Syst. II, Exp. Briefs*, vol. 68, no. 3, pp. 823–829, Mar. 2021.

[26] P. L. Lui, "Passive intermodulation interference in communication systems," *Electron. Commun. Eng. J.*, vol. 2, no. 3, pp. 109–118, 1990.

[27] *Passive Intermodulation (PIM) Handling for Base Stations (BS) (Release 12)*, document TR 37.808, V12.0.0, 3GPP, Sep. 2013.

[28] H. M. Karaca, "Passive inter-modulation sources and cancellation methods," *Eur. J. Res. Develop.*, vol. 2, no. 2, pp. 75–91, Jun. 2022.

[29] S. Sadjina, C. Motz, T. Paireder, M. Huemer, and H. Pretl, "A survey of self-interference in LTE-advanced and 5G new radio wireless transceivers," *IEEE Trans. Microw. Theory Techn.*, vol. 68, no. 3, pp. 1118–1131, Mar. 2020.

[30] D. S. Kozlov, A. P. Shitvov, A. G. Schuchinsky, and M. B. Steer, "Passive intermodulation of analog and digital signals on transmission lines with distributed nonlinearities: Modelling and characterization," *IEEE Trans. Microw. Theory Techn.*, vol. 64, no. 5, pp. 1383–1395, May 2016.

[31] R. Butler, A. Kurochkin, and N. Hugh, "Intermodulation products of LTE and 2G signals in multitechnology RF paths," *Bechtel Techn. J.*, vol. 2, pp. 1–12, Dec. 2009.

[32] D. Kozlov, A. P. Shitvov, S. Bulja, R. Lundy, P. Rulikowski, K. Nolan, and R. Enright, "Practical mitigation of passive intermodulation in microstrip circuits," *IEEE Trans. Electromagn. Compat.*, vol. 62, no. 1, pp. 163–172, Feb. 2020.

[33] F. Kearney and S. Chen, "Passive intermodulation (PIM) effects in base stations: Understanding the challenges and solutions," Analog Devices, Norwood, MA, USA, Tech. Rep., 51-03, Mar. 2017.

[34] T. S. D. Costa, "Characterization of passive intermodulation distortion in MultiBand FDD radio systems," M.S. thesis, KTH Roy. Inst. Technol., Stockholm, Sweden, Sep. 2019.

[35] J. R. Wilkerson, "Passive intermodulation distortion in radio frequency communication system," Ph.D. thesis, North Carolina State Univ., 2010.

[36] T. J. Rouphael, *Wireless Receiver Architectures and Design: Antennas, RF, Synthesizers, Mixed Signal, and Digital Signal Processing*. Amsterdam, The Netherlands: Elsevier, 2018.

[37] P. B. Kenington, *High Linearity RF Amplifier Design*. Norwood, MA, USA: Artech House, 2000.

[38] D. M. Pozar, *Microwave Engineering*. 4th ed. Hoboken, NJ, USA: Wiley, 2011.

[39] V. Golikov, S. Hienonen, and P. Vainikainen, "Passive intermodulation distortion measurements in mobile communication antennas," in *Proc. IEEE 54th Veh. Technol. Conf.*, Oct. 2001, pp. 2623–2625.

[40] T. Lähteensuo, "Linearity requirements in LTE-advanced mobile transmitter," M.S. thesis, Tampere Univ. Technol., Oct. 2012.

[41] A. J. Christianson, J. J. Henrie, and W. J. Chappell, "Higher order intermodulation product measurement of passive components," *IEEE Trans. Microw. Theory Techn.*, vol. 56, no. 7, pp. 1729–1736, Jul. 2008.

[42] R. Gerzaguet, L. Ros, F. Belvèze, and J.-M. Brossier, "Performance of a digital transmitter leakage LMS-based cancellation algorithm for multi-standard radio-frequency transceivers," *Digit. Signal Process.*, vol. 51, pp. 35–46, Apr. 2016.

[43] Y. Patenaude, J. Dallaire, F. Menard, and S. Richard, "Antenna PIM measurements and associated test facilities," in *IEEE Antennas Propag. Soc. Int. Symp. Dig. Held Conjunct*, Jul. 2001, pp. 620–623.

[44] M. Petek, "Modelling of passive intermodulation in RF systems," M.S. thesis, KTH Royal Inst. Technol., Stockholm, Sweden, Jun. 2020.

[45] S. Hienonen, "Studies on microwave antennas: Passive intermodulation distortion in antenna structures and design of microstrip antenna elements," Ph.D. thesis, Helsinki Univ. Technol., Jun. 2017.

[46] C. Vicente and H. L. Hartnagel, "Passive-intermodulation analysis between rough rectangular waveguide flanges," *IEEE Trans. Microw. Theory Techn.*, vol. 53, no. 8, pp. 2515–2525, Aug. 2005.
[47] C. Vicente, D. Wolk, H. L. Hartnagel, B. Gimeno, V. E. Boria, and D. Raboso, "Experimental analysis of passive intermodulation at waveguide flange bolted connections," *IEEE Trans. Microw. Theory Techn.*, vol. 55, no. 5, pp. 1018–1028, May 2007.
[48] J. Henrie, A. Christianson, and W. J. Chappell, "Prediction of passive intermodulation from coaxial connectors in microwave networks," *IEEE Trans. Microw. Theory Techn.*, vol. 56, no. 1, pp. 209–216, Jan. 2008.
[49] Y. Yamamoto and N. Kuga, "Short-circuit transmission line method for PIM evaluation of metallic materials," *IEEE Trans. Electromagn. Compat.*, vol. 49, no. 3, pp. 682–688, Aug. 2007.
[50] G. Macchiarella, G. B. Stracca, and L. Miglioii, "Experimental study of passive intermodulation in coaxial cavities for cellular base stations duplexers," in *Proc. 34th Eur. Microw. Conf.*, vol. 2, Oct. 2004, pp. 981–984.
[51] J. Wilkerson, K. Gard, and M. Steer, "Electro-thermal passive intermodulation distortion in microwave attenuators," in *Proc. Eur. Microw. Conf.*, Sep. 2006, pp. 157–160.
[52] J. R. Wilkerson, K. G. Gard, A. G. Schuchinsky, and M. B. Steer, "Electro-thermal theory of intermodulation distortion in lossy microwave components," *IEEE Trans. Microw. Theory Techn.*, vol. 56, no. 12, pp. 2717–2725, Dec. 2008.
[53] M. Z. Waheed, V. Lampu, A. Kiayani, M. Fleischer, L. Anttila, and M. Valkama, "Modeling and digital suppression of passive nonlinear distortion in simultaneous transmit—Receive systems," in *Proc. 56th Asilomar Conf. Signals, Syst., Comput.*, Oct. 2022, pp. 1339–1344.
[54] E. Dahlman and S. Parkvall, "NR—The new 5G radio-access technology," in *Proc. IEEE 87th Veh. Technol. Conf. (VTC Spring)*, Jun. 2018, pp. 1–6.
[55] H. Su, "Wide band TX leakage cancellation for FDD transceivers," Ph.D. thesis, Nat. Univ. Ireland, Jun. 2017.
[56] V. Lampu, L. Anttila, M. Turunen, M. Fleischer, J. Hellmann, and M. Valkama, "Air-induced passive intermodulation in FDD MIMO systems: Algorithms and measurements," *IEEE Trans. Microw. Theory Techn.*, vol. 71, no. 1, pp. 373–388, Jan. 2023.
[57] C. Lederer and M. Huemer, "Simplified complex LMS algorithm for the cancellation of second-order TX intermodulation distortions in homodyne receivers," in *Proc. Conf. Rec. Forty 5th Asilomar Conf. Signals, Syst. Comput. (ASILOMAR)*, Nov. 2011, pp. 533–537.
[58] A. Kiayani, L. Anttila, and M. Valkama, "Modeling and dynamic cancellation of TX-RX leakage in FDD transceivers," in *Proc. IEEE 56th Int. Midwest Symp. Circuits Syst. (MWSCAS)*, Aug. 2013, pp. 1089–1094.
[59] F. Chen, "Passive inter-modulation cancellation in FDD system," M.S. thesis, Lund Univ., Mar. 2017.
[60] D. Kozlov, S. Bulja, R. Lundy, P. Rulikowski, and J. J. Walsh, "Mitigation of passive intermodulation on planar microstrip circuits with distributed current-driven nonlinearities," in *Proc. 48th Eur. Microw. Conf. (EuMC)*, Sep. 2018, pp. 1029–1032.
[61] J. J. Henrie, A. J. Christianson, and W. J. Chappell, "Linear-nonlinear interaction and passive intermodulation distortion," *IEEE Trans. Microw. Theory Techn.*, vol. 58, no. 5, pp. 1230–1237, May 2010.
[62] J. Wannstrom. (Dec. 11, 2022). *Carrier Aggregation Explained*. Accessed: Oct. 23, 2023. [Online]. Available: https://www.3gpp.org/technologies/101-carrier-aggregation-explained
[63] *Multi-standard Radio Base Station (BS) Radio Frequency (RF) Requirements for Non-contiguous Spectrum Deployments (Release 10)*, document TS 37.802, V10.1.0, 3GPP, Sep. 2011.
[64] Q. Jin, J. Gao, H. Huang, and L. Bi, "Mitigation methods for passive intermodulation distortion in circuit systems using signal compensation," *IEEE Microw. Wireless Compon. Lett.*, vol. 30, no. 2, pp. 205–208, Feb. 2020.
[65] V. Lampu, L. Anttila, M. Turunen, M. Fleischer, J. Hellmann, and M. Valkama, "Air-induced PIM cancellation in FDD MIMO transceivers," *IEEE Microw. Wireless Compon. Lett.*, vol. 32, no. 6, pp. 780–783, Jun. 2022.
[66] E. Tsui, P. Maxwell, and W. Ye, "Facilitation of passive intermodulation cancellation via machine learning," U.S. Patent 10 601 456 B2, Mar. 24, 2022.
[67] V. Lampu, L. Anttila, M. Turunen, M. Fleischer, J. Hellmann, and M. Valkama, "Air-induced passive intermodulation in FDD networks: Modeling, cancellation and measurements," in *Proc. 55th Asilomar Conf. Signals, Syst., Comput.*, Oct. 2021, pp. 983–988.
[68] F. B. Mismar, "Intermodulation interference detection in 6G networks: A machine learning approach," in *Proc. IEEE 95th Veh. Technol. Conf.*, Jun. 2022, pp. 1–6.
[69] L. Niyonkuru, "Carrier aggregation intermodulation distortions in 4G and 5G mobile networks," Ph.D. thesis, Vrije Univ. Brussel, Mar. 2020.
[70] A. S. Tehrani, "Behavioral modeling of wireless transmitters for distortion mitigation," Ph.D. thesis, Chalmers Univ. Technol., 2012.
[71] A. S. Tehrani, H. Cao, S. Afsardoost, T. Eriksson, M. Isaksson, and C. Fager, "A comparative analysis of the complexity/accuracy tradeoff in power amplifier behavioral models," *IEEE Trans. Microw. Theory Techn.*, vol. 58, no. 6, pp. 1510–1520, Jun. 2010.
[72] P. L. Lui, "A study of intermodulation interference due to non-linearities in metallic structures," Ph.D. thesis, Univ. Kent Canterbury, 1990.
[73] S. D. Mitchell, "An investigation into the passive intermodulation properties of space qualified materials," Ph.D. thesis, Univ. Kent, 1997.
[74] L. Tian, H. Han, W. Cao, X. Bu, and S. Wang, "Adaptive suppression of passive intermodulation in digital satellite transceivers," *Chin. J. Aeronaut.*, vol. 30, no. 3, pp. 1154–1160, Jun. 2017.
[75] C. Xin, "Radio frequency circuits for wireless receiver front-ends," Ph.D. thesis, Texas A&M Univ., Aug. 2004.
[76] A. V. Oppenheim, R. W. Schafer, and J. R. Buck, *Discrete-Time Signal Processing*, 2nd ed. Englewood Cliffs, NJ, USA: Prentice-Hall, 1999.
[77] W. van Drongelen, *Signal Processing for Neuroscientists: Introduction to the Analysis of Physiological Signals*, 2nd ed. Cambridge, MA, USA: Academic Press, 2018.
[78] M. Schetzen, *The Volterra and Wiener Theories of Nonlinear Systems*. New York, NY, USA: Wiley, 1980.
[79] S. Bekleric, "Nonlinear prediction via Volterra series and applications to geophysical data," M.S. thesis, Univ. Alberta, 2008.
[80] M. Z. Waheed, D. Korpi, L. Anttila, A. Kiayani, M. Kosunen, K. Stadius, P. P. Campo, M. Turunen, M. Allén, J. Ryynänen, and M. Valkama, "Passive intermodulation in simultaneous transmit-receive systems: Modeling and digital cancellation methods," *IEEE Trans. Microw. Theory Techn.*, vol. 68, no. 9, pp. 3633–3652, Sep. 2020.
[81] M. Z. Waheed, P. P. Campo, D. Korpi, A. Kiayani, L. Anttila, and M. Valkama, "Digital cancellation of passive intermodulation in FDD transceivers," in *Proc. 52nd Asilomar Conf. Signals, Syst., Comput.*, Oct. 2018, pp. 1375–1381.
[82] K. Gharaibeh, "Assessment of various window functions in spectral identification of passive intermodulation," *Electronics*, vol. 10, no. 9, p. 1034, Apr. 2021. [Online]. Available: https://www.mdpi.com/2079-9292/10/9/1034
[83] J. Henrie, A. Christianson, and W. J. Chappell, "Engineered passive nonlinearities for broadband passive intermodulation distortion mitigation," *IEEE Microw. Wireless Compon. Lett.*, vol. 19, no. 10, pp. 614–616, Oct. 2009.
[84] A. Christianson, J. Henrie, and W. Chappell, "Matching network design for passive intermodulation distortion reduction," in *Proc. IEEE Antennas Propag. Soc. Int. Symp. (APSURSI)*, Jul. 2013, pp. 2247–2248.
[85] *Evolved Universal Terrestrial Radio Access (E-UTRA); User Equipment (UE) Radio Transmission and Reception (Release 18)*, document TS 36.101, V18.1.0, 3GPP, Mar. 2023.
[86] H.-T. Dabag, H. Gheidi, S. Farsi, P. S. Gudem, and P. M. Asbeck, "All-digital cancellation technique to mitigate receiver desensitization in uplink carrier aggregation in cellular handsets," *IEEE Trans. Microw. Theory Techn.*, vol. 61, no. 12, pp. 4754–4765, Dec. 2013.
[87] H.-T. Dabag, H. Gheidi, P. Gudem, and P. M. Asbeck, "All-digital cancellation technique to mitigate self-jamming in uplink carrier aggregation in cellular handsets," in *IEEE MTT-S Int. Microw. Symp. Dig.*, Jun. 2013, pp. 1–3.
[88] *Evolved Universal Terrestrial Radio Access (E-UTRA); Base Station (BS) Radio Transmission and Reception (Release 18)*, document TS 36.104, V18.1.0, 3GPP, Mar. 2023.
[89] Q. Jin, J. Gao, G. T. Flowers, Y. Wu, G. Xie, and L. Bi, "Modeling of passive intermodulation in connectors with coating material and iron content in base brass," *IEEE Trans. Microw. Theory Techn.*, vol. 67, no. 4, pp. 1346–1356, Apr. 2019.
[90] R. Wang, W. Cui, X. Chen, C. Bai, N. Zhang, and Y. Li, "Experimental analysis of passive intermodulation at TNC coaxial connectors," in *Proc. 11th Eur. Conf. Antennas Propag. (EUCAP)*, Mar. 2017, pp. 2383–2386.
[91] M. Wang, S. Li, R. Baldemair, J.-F. Cheng, F. Ghasemzadeh, M. Larsson, and J. Sköld, "Dynamic cancellation of passive intermodulation," U.S. Patent 9 026 064 B2, May 5, 2015.

[92] H. Jung and O. K. Tonguz, "Random spacing channel assignment to reduce the nonlinear intermodulation distortion in cellular mobile communications," *IEEE Trans. Veh. Technol.*, vol. 48, no. 5, pp. 1666–1675, Sep. 1999.
[93] E. A. Keehr and A. Hajimiri, "Successive regeneration and adaptive cancellation of higher order intermodulation products in RF receivers," *IEEE Trans. Microw. Theory Techn.*, vol. 59, no. 5, pp. 1379–1396, May 2011.
[94] X. Miao and L. Tian, "Digital cancellation scheme and hardware implementation for high-order passive intermodulation interference based on Hammerstein model," *China Commun.*, vol. 16, no. 9, pp. 165–176, Sep. 2019.
[95] H. Kamizuma, T. Masuda, and M. Onishi, "Third-order intermodulation product canceller for LTE base station receiver," in *Proc. 41st Eur. Microw. Conf.*, Japan, Oct. 2011, pp. 230–233.
[96] B. Jang, S. Im, C. Kim, and S. Hong, "Modeling of passive intermodulation distortion using the neural networks and the cubic Volterra filter," in *Proc. Int. Conf. Inf. Commun. Technol. Converg. (ICTC)*, Oct. 2019, pp. 1042–1046.
[97] B. Jang, S. Im, D. Lee, C. Kim, S. Hong, and J. Song, "PIMD signal modeling based on FTDNN," in *Proc. IEEE 2nd Int. Conf. Inf. Commun. Signal Process. (ICICSP)*, Sep. 2019, pp. 1–4.
[98] B. Jang, H. Kim, Y. Seo, S. Im, and S. Hong, "Mitigation of the third-order passive intermodulation distortion interference on uplink signal," in *Proc. Int. Conf. Electron., Inf., Commun. (ICEIC)*, Jan. 2019, pp. 1–3.
[99] J. C. Pedro and N. B. Carvalho, *Intermodulation Distortion in Microwave and Wireless Circuits*. Norwood, MA, USA: Artech House, 2003.
[100] S. S. Haykin, *Adaptive Filter Theory*. London, U.K.: Pearson, 2008.

TUHEEN AHMMED (Senior Member, IEEE) received the B.Sc. (Hons.) degree in electrical and electronic engineering from the Bangladesh Institute of Technology, Rajshahi, in 2002, and the M.B.A. degree from the University of South Dakota, Vermillion, SD, USA, in 2018. He is currently pursuing the M.A.Sc. degree in electrical and computer engineering with Carleton University. He is a Systems Developer with Ericsson Canada Inc. His research interests include passive intermodulation cancellation techniques, 5G radio development, and machine learning.

ADNAN KIAYANI (Member, IEEE) received the M.Sc. (Hons.) and D.Sc. degrees in electrical engineering from Tampere University, Tampere, Finland, in 2009 and 2015, respectively. From 2015 to 2018, he was a Postdoctoral Researcher with Tampere University. Since 2017, he has been a Radio System Designer with Ericsson AB, Stockholm, Sweden. His research interests include behavior modeling of RF systems and signal processing algorithms for flexible radio transceivers.

RAED M. SHUBAIR (Senior Member, IEEE) received the B.Sc. degree (Hons.) in electrical engineering from Kuwait University, Kuwait, in June 1989, and the Ph.D. degree (Hons.) in electrical engineering from the University of Waterloo, Waterloo, ON, Canada, in February 1993.

From 1993 to 2017, he was a Full Professor of electrical engineering with Khalifa University, Abu Dhabi. His current and past academic and research appointments also include the Massachusetts Institute of Technology (MIT), Cambridge, MA, USA, Harvard University, Cambridge, and the University of Waterloo. He is currently a Full Professor of electrical engineering with New York University (NYU) Abu Dhabi. He has more than 380 publications in the form of articles in peer-reviewed journals, papers in refereed conference proceedings, book chapters, and U.S. patents.

Dr. Shubair was a recipient of several international awards, including the Distinguished Service Award from the ACES Society, USA, and the MIT Electromagnetics Academy, USA. He also received the University of Waterloo Distinguished Doctorate Dissertation Award for the Ph.D. degree. He delivered more than 60 invited speaker seminars and technical talks at world-class universities and conferences. He served as an invited speaker with the U.S. National Academies of Sciences, Engineering, and Medicine Frontiers Symposium. He is the Founding Director of the IEEE UAE Distinguished Seminar Series Program, for which he was selected, along with Mohamed Al Hajri of MIT, for the 2020 IEEE UAE Award of the Year. He currently serves as the General Chair for IEEE WCNC 2024.

HALIM YANIKOMEROGLU (Fellow, IEEE) received the B.Sc. degree in electrical and electronics engineering from Middle East Technical University, Ankara, Turkey, in 1990, and the M.A.Sc. degree in electrical engineering and the Ph.D. degree in electrical and computer engineering from the University of Toronto, Canada, in 1992 and 1998, respectively.

Since 1998, he has been with the Department of Systems and Computer Engineering, Carleton University, Ottawa, Canada, where he is currently a Chancellor's Professor. He has given more than 110 invited seminars, keynotes, panel talks, and tutorials in the last five years. He has supervised or hosted more than 150 postgraduate researchers in the laboratory with Carleton University. His extensive collaborative research with industry resulted in 39 granted patents. His research interests include wireless communications and networks, with a special emphasis on non-terrestrial networks (NTN) in recent years.

Dr. Yanikomeroglu is a fellow of the Engineering Institute of Canada (EIC) and the Canadian Academy of Engineering (CAE). He is also a member of the IEEE ComSoc Governance Council, IEEE ComSoc GIMS, IEEE ComSoc Conference Council, and IEEE PIMRC Steering Committee. He received several awards for research, teaching, and service, including the IEEE ComSoc Satellite and Space Communications TC Recognition Award, in 2023, the IEEE ComSoc Fred W. Ellersick Prize, in 2021, the IEEE VTS Stuart Meyer Memorial Award, in 2020, and the IEEE ComSoc Wireless Communications TC Recognition Award, in 2018. He also received the Best Paper Award from the IEEE Competition on Non-Terrestrial Networks for B5G and 6G, in 2022 (grand prize), IEEE ICC 2021, and IEEE WISEE 2021 and 2022. He served as the general chair and the technical program chair for several IEEE conferences. He is also serving as the Chair for the Steering Committee of IEEE's Flagship Wireless Event and the Wireless Communications and Networking Conference (WCNC). He has also served on the editorial boards for various IEEE periodicals. He is a Distinguished Speaker of the IEEE Communications Society and the IEEE Vehicular Technology Society, and an Expert Panelist of the Council of Canadian Academies (CCA|CAC). He has also served on editorial boards of various IEEE periodicals.